A Head-Mounted Operating Binocular for Augmented Reality Visualization in Medicine—Design and Initial Evaluation

Wolfgang Birkfellner*, Michael Figl, Klaus Huber, Franz Watzinger, Felix Wanschitz, Johann Hummel, Rudolf Hanel, Wolfgang Greimel, Peter Homolka, Rolf Ewers, and Helmar Bergmann

***Abstract*—Computer-aided surgery (CAS), the intraoperative application of biomedical visualization techniques, appears to be one of the most promising fields of application for augmented reality (AR), the display of additional computer-generated graphics over a real-world scene. Typically a device such as a head-mounted display (HMD) is used for AR. However, considerable technical problems connected with AR have limited the intraoperative application of HMDs up to now. One of the difficulties in using HMDs is the requirement for a common optical focal plane for both the real-world scene and the computer-generated image, and acceptance of the HMD by the user in a surgical environment. In order to increase the clinical acceptance of AR, we have adapted the Varioscope (Life Optics, Vienna), a miniature, cost-effective head-mounted operating binocular, for AR. In this paper, we present the basic design of the modified HMD, and the method and results of an extensive laboratory study for photogrammetric calibration of the Varioscope's computer displays to a real-world scene. In a series of 16 calibrations with varying zoom factors and object distances, mean calibration error was found to be 1.24 $\pm$ 0.38 pixels or 0.12 $\pm$ 0.05 mm for a 640 $\times$ 480 display. Maximum error accounted for 3.33 $\pm$ 1.04 pixels or 0.33 $\pm$ 0.12 mm. The location of a position measurement probe of an optical tracking system was transformed to the display with an error of less than 1 mm in the real world in 56% of all cases. For the remaining cases, error was below 2 mm. We conclude that the accuracy achieved in our experiments is sufficient for a wide range of CAS applications.**

***Index Terms*—Augmented reality, binocular, head-mounted display, varioscope.**

Manuscript received November 15, 2000; revised May 21, 2002. This work was supported in part by the Austrian research foundation FWF under research Grant P12464-MED and the Jubilaeumsfonds der Oesterreichischen Nationalbank Project OeNB 8450. The CARCAS-Group is supported by the SNF-Grant "Computer Aided and Image Guided Medical Interventions CO-ME." The Associate Editor responsible for coordinating the review of this paper and recommending its publication was D. Hawkes. *Asterisk indicates corresponding author.*

*W. Birkfellner is with the CARCAS-Group at the Kantonsspital Basel, Switzerland. He is currently on leave from the Department of Biomedical Engineering and Physics at Vienna General Hospital (e-mail: wbirkfellner@uhbs.ch).

M. Figl, K. Huber, J. Hummel, W. Greimel, and P. Homolka are with the Department of Biomedical Engineering and Physics, General Hospital, University of Vienna, A-1090 Vienna, Austria.

F. Watzinger, F. Wanschitz, and R. Ewers are with the Department of Oral and Maxillofacial Surgery, Vienna General Hospital, University of Vienna, A-1090 Vienna, Austria.

R. Hanel is with the Department of Diagnostic Radiology, Division of Osteoradiology, Vienna General Hospital, University of Vienna, A-1090 Vienna, Austria.

H. Bergmann is with the Department of Biomedical Engineering and Physics General Hospital, University of Vienna, A-1090 Vienna, Austria. He is also with the Ludwig-Boltzmann Institute of Nuclear Medicine, A-1090 Vienna, Austria.

Digital Object Identifier 10.1109/TMI.2002.803099

I. Introduction

THE TERM "augmented reality" (AR) refers to the overlay of computer-generated graphics over a real-world scene. A special requirement of AR is the fact that the structure generated by computer graphics has to be linked to the viewed scenery, i.e., the perceived position of the scenery and the computer-generated object have to match. A typical application example is the guidance of a mechanic during aircraft maintenance. A head-mounted display (HMD) can be used to generate a virtual view for guiding the service engineer through the plane's blueprints during inspection. Besides using a display system that allows for merging real and virtual views, a second requirement is the accurate tracking of the position of the viewer relative to the viewed scene [1].

Medicine is a field where the potential of possible applications appears to be tantalizing. The idea of providing X-ray vision to the physician is as old as medical imaging itself; realizing this goal in a way that is acceptable for the potential clinical end-user is, however, a major technical challenge. Computer-aided surgery (CAS), the guidance of the surgeon by means of intraoperative image processing, is an ideal field for AR since CAS provides all the basic technologies for AR such as three-dimensional (3-D) image information for deriving a virtual scenery and position tracking of the viewed objects (typically the patient or the surgical tool). The clinical benefit is the fact that the surgeon can concentrate on the operating field rather than looking at a monitor. Among the technical problems connected to the clinical application of AR are as follows

- The joint display of virtual and real scenery in the HMD which is difficult to achieve in a simple HMD design where the only optical element in the viewer's optical path is a simple beamsplitter. From the basic principles of geometrical optics, it follows that since the object distance of the virtual scenery reflected on the semi-transparent beamsplitter is different from the object distance of the real-world scenery, a common focus cannot be achieved by the viewer's eye. Either the virtual or the real-world view, therefore, appear unfocused. Placing a beamsplitter before the viewer's eye is, however, the most common design for commercially available HMDs.
- The acceptance of the HMD by physicians. Clinical experience with CAS clearly shows that an additional cumbersome device such as a bulky HMD will not find a place in the operating room.

0278-0062/02$17.00 © 2002 IEEE

• The registration of the virtual view and the real world which has to be maintained at all times within the accuracy requirements of the specific CAS application. This makes exact calibration of the HMD, i.e., the precise determination of the projective transformation between 3-D-coordinates and the HMD's display coordinates, and sophisticated real time tracking of the HMD necessary [1]. Otherwise, inaccuracies as well as simulator sickness are inevitable [2].

A method to overcome these difficulties is the integration of the AR-display system into a well-accepted surgical tool such as the operating microscope [3]. First of all, the usage of a complex optical instrument instead of a simple beamsplitter allows for merging virtual and real views in a common focal plane, thus avoiding the problem of focusing both scenes at the same time. Next, the operating microscope is a well-accepted surgical tool. Finally, the operating microscope is mounted to a stable gantry, therefore, the requirements for real time tracking are somewhat relaxed. While an operating microscope with the capability of merging real and virtual views is not a HMD, this approach appears to be a valuable method to introduce AR in clinical routine. However, the use of an operating microscope has limitations. While it is widely used in neurosurgery, which was also the first medical specialty to benefit from CAS, it is not available in all operating rooms, and many other surgical procedures do not utilize such a device. Introducing an expensive and bulky operating microscope for the sole purpose of AR appears also infeasible from an economical point of view.

Using a conventional HMD or display devices such as a semi-transparent panel suffer from the problem of not providing a common focal plane [4]. Video-based solutions consisting of a miniature monitor and a miniature video camera have also been explored [5] but suffer from additional weight and parallax effects as well as reduced visual quality of the real world scene.

This paper presents an alternative approach to solve the aforementioned problems of AR visualization. We have adapted a commercial miniature head-mounted operating binocular for stereoscopic AR visualization. The design of the system and a first assessment of the accuracy achievable with a standard photogrammetric calibration method for various zoom factors and working distances of the HMD constitute the content of this paper.

II. Materials and Methods

A. The Varioscope AR

The Varioscope is a head-mounted, lightweight operating binocular developed and produced by Life Optics, Vienna, Austria (Available at *http://www.lifeoptics.com*). It features autofocus with automatic parallax correction (operating range: approximately 300–600 mm) and zoom (magnification range 3.6–7.2×). Parallax correction is necessary since the short operating range would otherwise inevitably lead to double images due to the parallax between left and right eye; in the current version of the Varioscope, merging the optical axes of the left and right tube is achieved by moving the tubes in- and outwards. The overall weight of the Varioscope is about 300 grams. The physical dimensions of the base instrument are 73 × 120 × 64 mm (W/L/H). Current clinical applications of this instrument include plastic and reconstructive surgery, oral and cranio-maxillofacial surgery, and orthopedics. In principle, it replaces a fix-focus operating binocular.

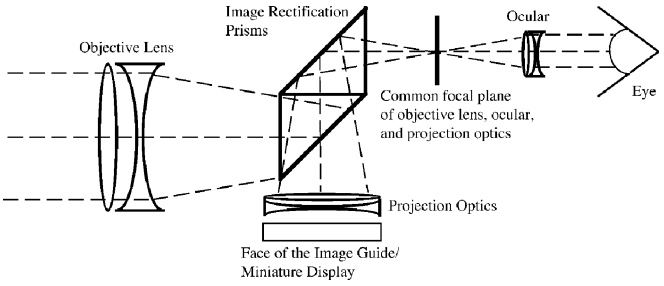

Fig. 1. The principle of image overlay in the Varioscope AR. An additional image from a miniature computer display is being projected into the focal plane of the Varioscope's objective lens. The merged image can be viewed through the ocular of the Varioscope.

This commercially available device was modified for AR visualization in close cooperation with the manufacturer and Docter Optics, Vienna, Austria; we refer to the prototype as the Varioscope AR. Since the optical properties of the Varioscope are the same as of an astronomical telescope, the insertion of image rectification prisms into the optical path is necessary; this offers a convenient way to add the beamsplitters for merging the computer-images and the optical view as captured by the lens of the Varioscope. One face of the image rectification prism was covered with a thin semi-transparent layer acting as a beamsplitter. Due to the design of this layer, the computer-generated and real images are mixed at a ratio of 20/60, whereas 20% of the incident light are lost in the current prototype. In spite of the loss of image brightness, the perception of the image remains almost unchanged due to the low focal ratio of the Varioscope.

The computer-generated images are displayed on two miniature LCD displays with VGA resolution (AMEL640.480.24, 640 × 480 pixels, Planar Microdisplays Inc., Beaverton, OR). The displays have an active area of 15.5 × 11.4 $mm^2$and a luminance of 1700 cd/m^2. The high brightness of the displays allows for projecting the image without additional background illumination. In the original prototype used for the experiments, the image size was reduced with a commercially available reduction lens (3.4/16, Docter Optics) by a factor of −0.67. The image with 8 × 10 mm^2 was transferred through a flexible image guide with 800 × 1000 fibers (IG 163, Schott Fiberoptics, Southbridge, MA) to a specially designed projection lens of the Varioscope AR. The core distance of the fibers was 10 μm. In order to get a more compact design (Fig. 2), the projection optics were changed immediately after the experiments described in this paper so that the image guides became obsolete. The optical properties, however, remained the same. The projection optics is designed in such a manner that the eye lens (or ocular) of the Varioscope magnifies both the image from the main lens and from the projection optics, both of which provide an image in the focal plane of the main lens (Fig. 1). By exploiting this specific feature of the Varioscope, we were able to solve the problem of providing a commonly focused view of real and virtual scenes.

Fig. 2. A photograph of the prototype of the Varioscope AR. Visible are (a) the base instrument and (b) the housing for the projection optics with the miniature displays. Since the Varioscope AR is designed for stereoscopic vision, two display systems are connected to the Varioscope AR.

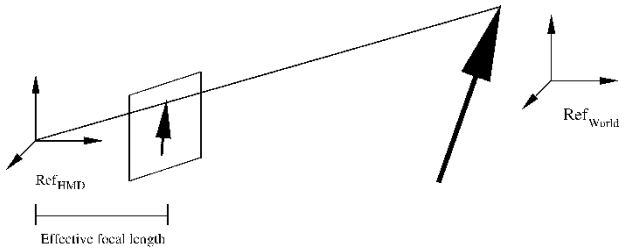

Fig. 3. Illustration of the parameters to be determined by the photogrammetric calibration routine. In addition to the rigid body transformation between the coordinate systems $\mathrm{Ref}_{\mathrm{World}}$ and $\mathrm{Ref}_{\mathrm{HMD}}$, the effective focal length, a projection parameter that originates from the underlying pinhole-camera model, has to be determined.

B. Photogrammetric Calibration

The basic problem of relating 3-D position information to the two-dimensional (2-D) coordinate system of the HMD's display is the photogrammetric calibration. We have decided to employ Tsai's algorithm for camera calibration described in detail in [6]; an implementation of this algorithm by R. Willson available in the internet under *http://www.cs.cmu.edu/~rgw/TsaiCode.html* was used [7]. We adopted parts of that code to accommodate our requirements. In particular, we used a version of the algorithm that allows the derivation of the parameters for projective transformation by measuring a set of coplanar real world coordinates. In this case, it is necessary to ensure that the image plane of the optical system and the calibration grid are not parallel, a condition which is easy to fulfill. This is necessary in order to achieve clear separation between the parameters of effective focal length and the translation transformation between the coordinate system of the HMD and the grid (see [6] and Fig. 3).

Basically, the algorithm determines a transformation from 3-D world coordinates $\vec{r}$ to 2-D screen coordinates $\vec{d}$. Eleven parameters are needed to compute the transformation from world coordinates to the display coordinate system. These parameters are:

- Six *extrinsic* parameters describing the global rigid-body transformation relating the world coordinate system $\mathbf{Ref}_{\mathrm{World}}$ to the coordinate system $\mathbf{Ref}_{\mathrm{HMD}}$ of the display. These are the three Euler angles [8] describing the spatial orientation of the display's coordinate system, and three translation parameters describing the location of the coordinate system's origin. In our case, the orientation of the coordinate system is described in terms of a rotation matrix $\mathbf{R}$ derived from the Euler angles, and a 3-D translation vector $\vec{T}$.
- Five *intrinsic* parameters describing the projective properties of the display. These parameters are as follows.

  — f, the effective focal length of the optical system.

  — κ_1, the lens distortion coefficient. This quantity takes the residual optical error of geometrical distortion in the HMD's main lens into account.

  — s_x, the uncertainty scale factor, a quantity that takes the finite size of the display's pixel elements as well as other sources of error into account. This quantity was not used in our implementation since it turned out that it shows no measurable influence on the calibration.

  — C_x and C_y, the coordinates of the display's center. These parameters were determined manually by positioning a crosshair at the center of the HMD's field-of-view.

The intrinsic parameters as well as the transition from the world-coordinate system to the display-coordinate system are described in detail in [6]. The algorithm was implemented in ANSI-C for a Sun UltraSPARC 10 (Sun Microsystems, Palo Alto, CA) and an Intel based PC running SuSE Linux 6.4 (SuSE GmbH, Nürnberg, Germany). A graphical user interface (GUI) for the algorithm was programmed using Tcl/Tk 8.0 [9].

C. Experimental Procedure

The Varioscope AR was mounted to an optical table (Fig. 4) together with an aluminum plate containing a rectangular grid with 2.5-mm diameter holes and a 6-mm grid constant (Fig. 5). The grid was machined with 0.03-mm positioning accuracy. In our framework the calibration algorithm requires a set of coplanar world coordinates; the coordinate system was chosen in such a manner that the z-axis of the coordinate system is normal to the grid's plane, therefore, the coordinate-vector $\vec{r}$ of the grid was given as $\vec{r} = (x\ y\ 0)^T$.

The GUI used by the calibration program consists of a window with the exact dimensions (640 $\times$ 480 pixels) of the HMD's display. A crosshair can be freely moved in this window by a mouse positioned to any location $\vec{d}_i$ on the display. When taking a measurement, the crosshair was aimed at the center of a gridpoint on the calibration grid to obtain a position vector $\vec{d}_i$ in pixel units. The corresponding 3-D coordinate $\vec{r}_i$ was obtained by counting the gridpoints relative to the (arbitrary, but preselected) center of the grid's coordinate system and multiplying the values for the x and y grid positions with the grid constant, with z being zero for any point. Both the 2-D screen coordinates $\vec{d}_i$ and the corresponding 3-D grid locations $\vec{r}_i$ were recorded.

Sixteen measurement series with varying zoom factors and different distances between optics and grid were performed. Since the Varioscope does not have discrete zoom factors, we used the minimum zoom, the maximum value, and two intermediate factors. The number of acquired points for a calibration depended on the zoom-dependent field-of-view of the Var-

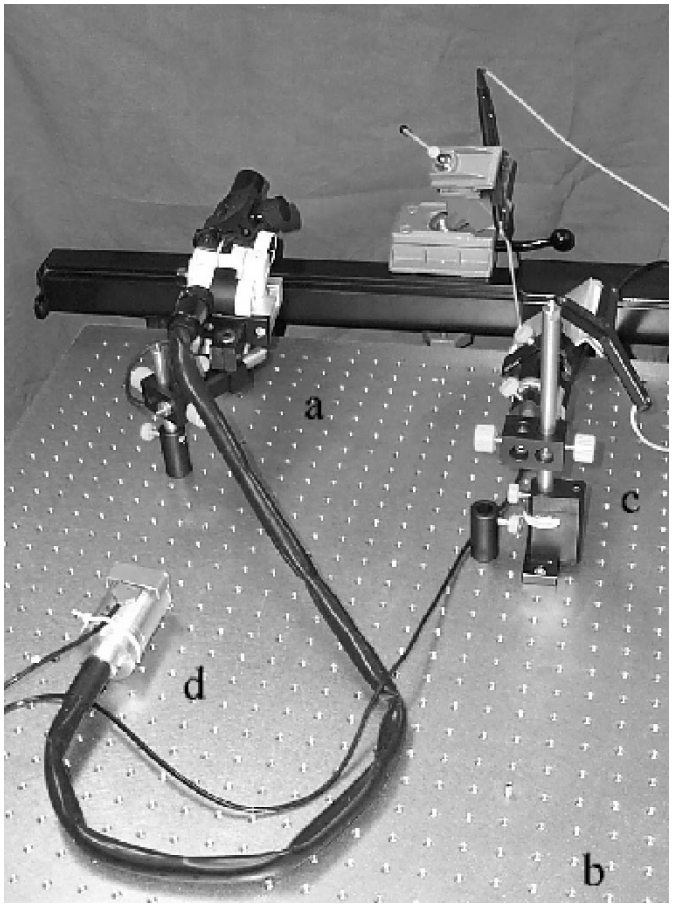

Fig. 4. Experimental setup for determination of the photogrammetric registration parameters. (a) The Varioscope AR was mounted to (b) an optical table. During the measurements, a crosshair at a defined 2-D screen position $\vec{d}_i$ is displayed on the HMD by the (d) miniature display system. The crosshair was aimed at the center of a grid point on (c) the calibration grid, and the 3-D coordinate of the gridpoint $\vec{r}_i$ is recorded. See Fig. 5 for a detailed view of the calibration grid. In this photograph, the first prototype of the Varioscope AR with image guides is shown. These were removed in the current prototype without changing the optical properties of the display system.

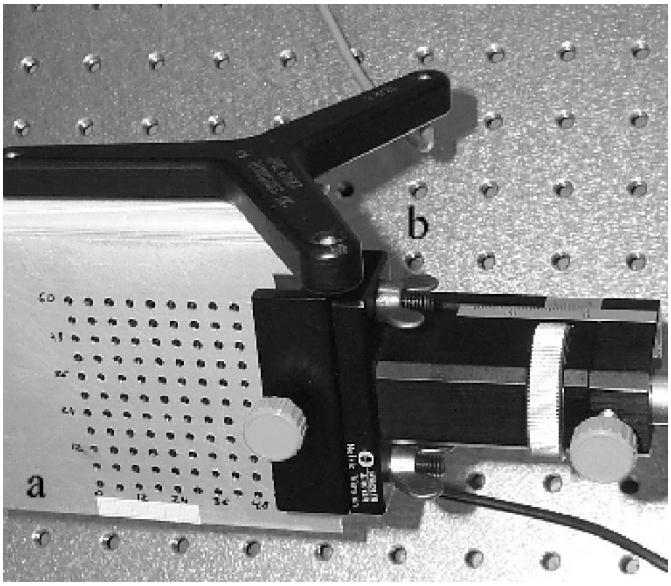

Fig. 5. (a) The calibration grid used for calibrating the HMD using Tsai's camera calibration algorithm. The grid was made using a high precision mill; each hole has a diameter of 2.5 mm. The grid constant is 6 mm. Furthermore, (b) an optical probe with three LED elements for tracking the grid's coordinate system can be seen.

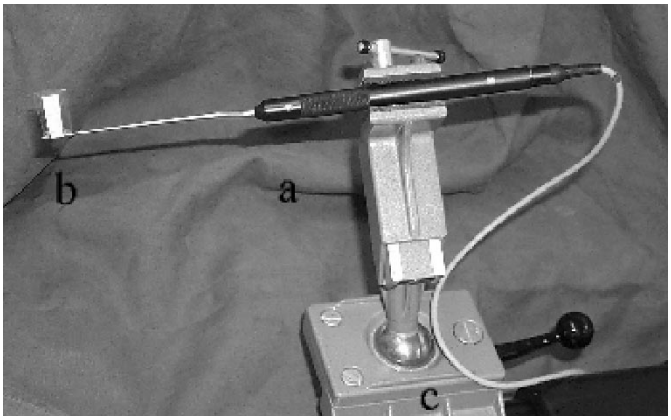

Fig. 6. (a) The surgical bayonet probe used for determination of the success of the HMD's calibration. Attached to (b) the probe's tip is a small ruler which allows for measuring the difference between the visual position of the probe's tip and its position after transformation to the HMD's display in millimeters. (c) For flexible positioning, the probe was fixed with a small vise to the optical table.

ioscope; they ranged from 30 to 110. Four measurement series were taken for each zoom factor. Also, four different distances of the grid from the HMD were used. The distance between HMD and grid was determined using a measuring tape. The grid's distance to the HMD was increased for each measurement by 50 mm, starting from an initial distance of approximately 200 mm. The scale factor between the display and the world coordinates was calibrated by displaying a bar of 100-pixel length on the Varioscope's display, the real world length of which was determined visually with a ruler on the grid plate. The average and maximum registration error as computed by the photogrammetric calibration algorithm was recorded; the scale calibration was used to compute the registration error in millimeters.

Furthermore, the effect of correction for the optical system's radial distortion was assessed. Tsai's algorithm allows the radial distortion in an optical system to be determined; a function for transforming 3-D world coordinates to display coordinates whilst taking distortion into account is given in [6]. Since we planned to display a virtual scenery by using the OpenGL graphics library [10], it was important to determine whether radial distortion was an important issue in the Varioscope AR or not. OpenGL supports perspective rendering, but radial warping of the viewed scenery to compensate for radial distortion caused by the Varioscope's optics would be difficult to implement [11]. If it were possible to neglect radial distortion the task of porting the graphics display to OpenGL would greatly be simplified.

Finally, we tested whether the projective transformation calculated by the photogrammetric calibration program transformed points which are in the coordinate system of the grid but not in the grid plane to an appropriate position on the HMD's display. For this purpose, a position measurement probe of an optical tracking system commonly used in CAS (Flashpoint 5000, Image Guided Technologies Inc., Boulder, CO, [12], [13]) was attached to the grid (Fig. 5). The technical accuracy of the tracker is better than 1 mm [14]. The tip of a

TABLE I
OPTICAL PARAMETERS AND SETTINGS FOR 16 CALIBRATION RUNS. FROM THE 16 MEASUREMENTS, FOUR WERE MADE FOR EACH OF THE FOUR CHOSEN ZOOM FACTORS (SECOND COLUMN). THE NUMBER OF POINTS MEASURED FOR DERIVING A CALIBRATION WAS RECORDED IN THE THIRD COLUMN. THE FOURTH COLUMN CONTAINS THE APPROXIMATE DISTANCE BETWEEN THE CALIBRATION GRID AND THE HMD. THE SCALE OF THE IMAGE AS PERCEIVED IN THE VARIOSCOPE ARE FOUND IN THE FIFTH COLUMN. FINALLY, THE EFFECTIVE FOCAL LENGTH, THE AVERAGE AND MAXIMUM CALIBRATION ERROR, AND THE LENS DISTORTION COEFFICIENT κ_1 AS DETERMINED BY THE ALGORITHM, ARE IN COLUMNS SIX TO NINE. AS OPPOSED TO THE SETUP VALUES IN COLS. 1 TO 5, THESE VALUES REPRESENT RESULTS FROM THE CALIBRATION MEASUREMENTS. LENS DISTORTION WAS TAKEN INTO ACCOUNT FOR COMPUTING THE CALIBRATION ERROR

Meas. #	Zoom	# of Points	Distance Grid–Image Plane (mm)	Scale $\left(\frac{\text{mm}}{\text{pixel}}\right)$	Effective focal length (mm)	Mean Calibration Error (pixel)	Maximum Calibration Error (pixel)	κ_1 $\left(\frac{1}{\text{mm}^2}\right)$
1	Min.	42	170	0.09	**33.3**	**1.76**	**4.55**	**0.0002**
2	Min.	39	220	0.09	**31.3**	**1.96**	**5.35**	**0.0004**
3	Min.	87	270	0.11	**30.6**	**1.12**	**3.17**	**-0.0003**
4	Min.	97	320	0.13	**30.2**	**0.88**	**2.12**	**-0.0003**
5	Med. I	51	250	0.08	**43.5**	**0.92**	**2.79**	**-0.0007**
6	Med. I	101	300	0.11	**42.6**	**1.02**	**3.26**	**-0.0009**
7	Med. I	93	350	0.13	**41.1**	**0.93**	**2.22**	**-0.0005**
8	Med. I	110	400	0.16	**40.3**	**1.71**	**4.14**	**0.0003**
9	Med. II	30	250	0.07	**60.4**	**1.31**	**2.67**	**-0.0007**
10	Med. II	37	280	0.08	**55.9**	**1.28**	**2.97**	**-0.004**
11	Med. II	45	320	0.09	**54.8**	**1.07**	**3.09**	**-0.0005**
12	Med. II	61	370	0.10	**49.7**	**1.68**	**4.15**	**-0.0003**
13	Max.	34	310	0.07	**64.7**	**1.31**	**3.33**	**-0.0005**
14	Max.	51	360	0.08	**60.7**	**1.43**	**4.99**	**-0.009**
15	Max.	81	410	0.11	**59.1**	**0.80**	**2.90**	**-0.001**
16	Max.	82	460	0.11	**61.1**	**0.69**	**1.66**	**-0.0007**

surgical bayonet probe also equipped with LEDs (Fig. 6) was used as a target and moved in the grid coordinate system in the focal range (approximately 50 mm) of the Varioscope. The reference coordinate system of the grid's position measurement probe (Fig. 5) was transformed to the grid's coordinate system by deriving a rigid-body transformation with a point-to-point registration algorithm [15] also widely used in CAS [14]. The fiducial registration error [16], given the euclidean error after transforming fiducial positions used for finding the transformation back to their original coordinate system, was found to be 0.7 mm. By reading the bayonet probe's position into the workstation driving the HMD (see [17] for a detailed description of the computer's interface to the tracker) and transforming these readings to the grid's coordinate system, a coordinate $\vec{r}$ was derived which was then transformed to the HMD's display coordinates. The error was assessed in millimeters by comparing the position of the probe's tip as seen through the Varioscope with the position of the tip displayed as a cross by the HMD. The points selected were approximately equally distributed throughout the volume limited by the field of view of the Varioscope AR and the focal range. Comparison was done by attaching a small ruler to the probe so that the differences could be directly read out visually in units of millimeters (Fig. 6). The error Δ given as the visual difference between displayed and true tip position was classified in three intervals of $\Delta \leq 1$ mm, 1 mm $\leq \Delta \leq 2$ mm, and $\Delta > 2$ mm. Three measurements were taken for each calibration, resulting in a total of 48 measurements for the 16 calibration procedures.

III. RESULTS

The experimental parameters such as the number of measured point coordinates, distance between grid and HMD, and scale for the 16 calibration experiments were collected in Table I. The resulting intrinsic parameters for the projective transformation from world coordinates to display coordinates (effective focal length and distortion coefficient κ_1) as calculated by the camera calibration algorithm were also collected in this table. Fig. 7 shows a graph visualizing the relationship between effective focal length and the approximate distance between the HMD and the grid. Average error of the calibration as determined by transforming the 3-D grid coordinates to the two-dimensional (2-D) display coordinates using the found projection parameters accounted for 1.24 ± 0.38 pixels or 0.12 ± 0.05 mm, respectively, when applying the radial distortion correction, and for 1.58 ± 0.34 pixels or 0.15 ± 0.04 mm, respectively, without distortion correction. Maximum error was found to be 3.33 ± 1.04 pixels and 0.33 ± 0.12 mm, respectively, with correction and 4.24 ± 1.22 pixels or 0.42 ± 0.14 mm without distortion correction. Detailed results for the calibration errors determined with and without distortion correction are shown in Fig. 8. The data presented in this diagram show that for each zoom factor and each distance between the HMD and the viewed object (i.e., the calibration grid), distortion correction does not significantly influence the performance of the HMD when projecting the 3-D world coordinates to the display coordinates.

Out of the 48 measurements carried out with the surgical bayonet probe, with positions outside the plane of the calibration

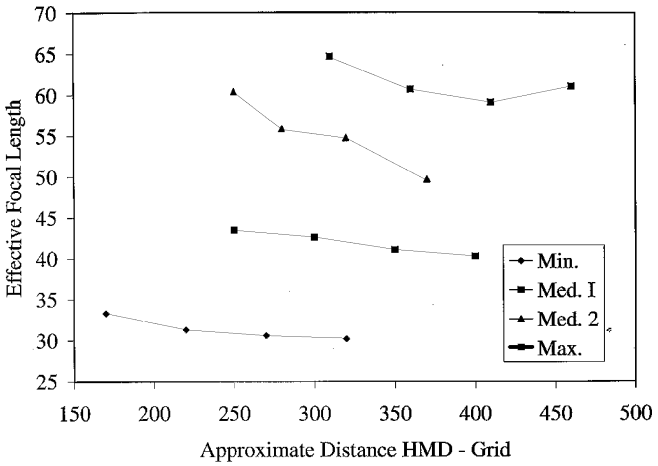

Fig. 7. The effective focal length for various zoom factors (Minimal, Maximal, and two zoom factors Medium 1 and Medium 2 in between) as a function of the approximate distance between HMD and the grid.

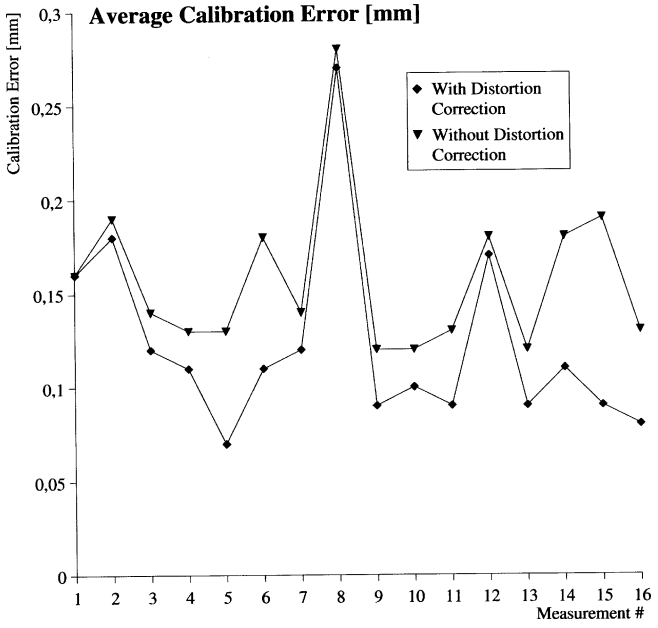

Fig. 8. The average calibration error for the 16 calibration runs; the error was transformed to millimeters using the actual scale factor for each measurement. In the case of the first graph, the geometric radial distortion of the Varioscope was taken into account using the found distortion parameters. In the second graph, distortion was omitted. The number of point measurements used for each calibration is given in Table I.

grid, the error Δ between the visual position and the position displayed in the HMD was less than 1 mm in 56% of all measurements, and in the remaining 44% less than 2 mm. No error Δ beyond 2 mm was encountered.

IV. Discussion and Conclusion

The development of the Varioscope AR is an ongoing research effort; important features like the automatic selection of the appropriate set of calibration parameters from given internal optical parameters like zoom and focal distance are still to be realized. However, our experiments show that an accurate calibration of a head mounted operating binocular can fulfill the accuracy requirements of CAS, which are technically limited by the resolution of the imaging modality used for preoperative planning. At the moment, conventional CT-scanners found in clinical practice can provide images with a resolution of approximately $0.25 \times 0.25 \times 1.00$ mm^3. Especially, the error Δ obtained for the measurements using the surgical bayonet probe and the optical tracking system compares well with the overall accuracy of the tracking system. As shown in Fig. 8, correction for radial distortion does not significantly improve the calibration accuracy, especially when comparing these values with a navigation system's errors [14]. Further improvements are, however, still possible, for instance by increasing the number of gridpoints for calibration. Furthermore we have established a steady relationship between the distance of the viewed object (the grid) and the effective focal length (Fig. 7). Therefore, accurate measurement of the Varioscope's current zoom factor in real time, e.g., by attaching a linear encoder to the Varioscope's internal mechanics, can be used to unambiguously assign and use the correct calibration dataset. This has been performed previously for operating microscopes [3]; due to the fact that in the case of the Varioscope AR and operating binoculars in general the field-of-view and the depth-of-field is larger, we do not expect considerable problems when implementing this. In fact, a survey of the commercial literature available from three leading manufacturers of operating microscopes revealed a field-of-view ranging from 150 mm down to 7 mm. Comparing this with the data given in [18], the field-of-view of an operating binocular ranges between 176.6 and 38 mm. The Varioscope with its field-of-view between 140 and 33 mm, therefore, belongs to the latter category. Currently, the Varioscope AR can be used for further experimental work without automatic focus and zoom adaptation like a normal operating binocular.

As a consequence, calibration for a given zoom factor and a given object distance (which also can be determined using the autofocus system of the Varioscope) needs to be carried out only once and does not have to be repeated for each use of the Varioscope AR in the operating theater. The modifications necessary for zoom and focus are currently under way but were not yet fully implemented.

The system will first be connected to VISIT, a navigation system developed at our hospital [14], [17]. VISIT includes an optical tracker which will be used also to track the HMD. Computer-aided insertion of endosteal implants in the skull for prosthetic and reconstructive purposes [14], [19], [20] have been the first clinical applications of VISIT; the basic task of the system is to guide the surgeon in the operating theater to an implant position planned preoperatively on a high-resolution CT scan. The planned and the actual drill position are visualized on the real-time system by means of OpenGL rendering; this was done using the freely available library Mesa 3.0 (http://www.mesa3d.org). The accuracy of VISIT was found to be 1.3 ± 0.3 mm [14]. The results of this study compare well with these results, thus the intraoperative use of the Varioscope AR is straightforward and will consist of displaying the actual drill position relative to the planned implant position, overlaying the real world display of the operation field with the computer graphics.

A system for connecting the Varioscope AR to the navigation system has already been developed. A high-performance workstation running VISIT interfaces to an Intel-based PC connected

to the HMD and the optical tracker; therefore, all position information regarding the HMD, the patient, and the surgical tools is at hand. Despite the fact the Varioscope AR is still under development, the large depth-of-field of the system allowed for first cadaver studies [21]. Besides the further development of the system, preclinical and clinical evaluation at various surgical departments form the current focus of our work.

ACKNOWLEDGMENT

The authors wish to thank Dr. M. Lehrl, Ing. K. Portschy, Ing. H. Wallner, and their colleagues at Life Optics, for the close cooperation and the excellent relationship. The would also like to thank W. Piller (Ludwig-Boltzmann Institute of Nuclear Medicine, Vienna, Austria), S. Baumgartner, A. Taubeck, A. Gamperl, P. Stadlmaier, and W. Zawodsky (Department of Biomedical Engineering and Physics, University of Vienna, Vienna, Austria) for valuable expertise and assistance provided in the manufacturing of the hardware for the Varioscope AR. They would also like to thank Dr D. Legenstein (Institute for Flexible Automation, Technical University Vienna) for valuable information provided on camera calibration in general. Finally, the authors would like to acknowledge that this project would not have been feasible without the input from their colleagues at various clinical departments at Vienna General Hospital. *Varioscope* is a registered trademark of Life Optics, Vienna.

REFERENCES

[1] R. T. Azuma, "A survey of augmented reality," *Presence: Teleoperators Virtual Environ.*, vol. 6, no. 4, pp. 355–386, 1997.

[2] S. Bangay and L. Preston, "An investigation into factors influencing immersion in interactive virtual reality environments," *Stud. Health Technol. Inform.*, vol. 58, pp. 43–51, 1998.

[3] P. J. Edwards, A. P. King, C.R. Maurer, Jr., D. A. de Cunha, D. J. Hawkes, D. L. G. Hill, R. P. Gaston, M. R. Fenlon, A. Jusczyck, A. J. Strong, C. L. Chandler, and M. L. Gleeson, "Design and evaluation of a system for microscope-assisted guided interventions (MAGI)," *IEEE Trans. Med. Imag.*, vol. 19, pp. 1082–1089, Nov. 2000.

[4] F. Watzinger, F. Wanschitz, M. Rasse, W. Millesi, C. Schopper, J. Kremser, W. Birkfellner, K. Sinko, and R. Ewers, "Computer-aided surgery in distraction osteogenesis of the maxilla and mandible," *Int. J. Oral Maxillofac. Surg.*, vol. 28, no. 3, pp. 171–175, 1999.

[5] C. R. Maurer Jr., F. Sauer, B. Hu, B. Bascle, B. Geiger, F. Wenzel, F. Recchi, T. Rohlfing, C. M. Brown, R. S. Bakos, R. J. Maciunas, and A. Bani-Hashemi, "Augmented reality visualization of brain structures with stereo and kinetic depth cues: System description and initial evaluation with head phantom," in *Proc. SPIE*, K. S. Mun, Ed., 2001, vol. 4319, Medical Imaging 2001: Visualization, Display, and Image Guided Procedures, pp. 445–456.

[6] R. Y. Tsai, "A versatile camera calibration technique for high-accuracy 3-D machine vision metrology using off-the-shelf TV cameras and lenses," *IEEE Trans. Robot. Automat.*, vol. RA-3, pp. 323–344, 1987.

[7] R. G. Willson, "Modeling and calibration of automated zoom lenses," Ph.D. dissertation, Robot. Inst., Carnegie Mellon Univ., Pittsburg, PA, 1994. [Online]. Available: http://www.cs.cmu.edu/~rgw.

[8] K. W. Spring, "Euler parameters and the use of quaternion algebra in the manipulation of finite rotations," *Mech. Mach. Theory*, vol. 21, no. 5, pp. 365–373, 1986.

[9] J. K. Ousterhout, *Tcl and the Tk Toolkit*. Reading, MA: Addison-Wesley, 1994.

[10] OpenGL Architecture Review Board, *OpenGL Reference Manual*, 2nd ed, R. Kempf and C. Frazier, Eds. Reading, MA: Addison-Wesley, 1997.

[11] B. A. Watson and L. F. Hodges, "Using texture maps to correct for optical distortion in head-mounted displays," in *Proc. VRAIS '95*, pp. 172–178.

[12] W. Birkfellner, F. Watzinger, F. Wanschitz, R. Ewers, and H. Bergmann, "Calibration of tracking systems in a surgical environment," *IEEE Trans. Med. Imag.*, vol. 17, pp. 737–742, Oct. 1998.

[13] S. A. Tebo, D. A. Leopold, D. M. Long, and S. J. Zinreich, "An optical 3-D digitizer for frameless stereotactic surgery," *IEEE Comput. Graphics Applicat.*, pp. 55–64, Jan 1996.

[14] W. Birkfellner, P. Solar, A. Gahleitner, K. Huber, F. Kainberger, J. Kettenbach, P. Homolka, M. Diemling, G. Watzek, and H. Bergmann, "In-vitro assessment of a registration protocol for image guided implant dentistry," *Clin. Oral Implants Res.*, vol. 12, no. 1, pp. 69–78, 2001.

[15] B. K. P. Horn, "Closed form solution of absolute orientation using unit quaternions," *Soc. Amer. A*, vol. 4, no. 4, pp. 629–642, 1987.

[16] J. M. Fitzpatrick, J. B. West, and C. R. Maurer, "Predicting error in rigid-body point-based registration," *IEEE Trans. Med. Imag.*, vol. 17, pp. 694–702, Oct. 1998.

[17] W. Birkfellner, K. Huber, A. Larson, D. Hanson, M. Diemling, P. Homolka, and H. Bergmann, "A modular software system for computer-aided surgery and its first application in oral implantology," *IEEE Trans. Med. Imag.*, vol. 19, pp. 616–620, June 2000.

[18] J. M. Baker and R. A. Meals, "A practical guide to surgical loupes," *J. Hand Surg.*, vol. 22A, pp. 967–974, 1997.

[19] F. Watzinger, W. Birkfellner, F. Wanschitz, W. Millesi, C. Schopper, K. Sinko, K. Huber, H. Bergmann, and R. Ewers, "Positioning of dental implants using computer-aided navigation and an optical tracking system: Case report and presentation of a new method," *J. Craniomaxillofac. Surg.*, vol. 27, no. 4, pp. 77–81, 1999.

[20] F. Watzinger, W. Birkfellner, F. Wanschitz, F. Ziya, A. Wagner, J. Kremser, F. Kainberger, K. Huber, H. Bergmann, and R. Ewers, "Placement of endosteal implants in the zygoma after maxillectomy: A cadaver study using surgical navigation," *Plast. Reconstr. Surg.*, vol. 107, no. 3, pp. 659–667, 2001.

[21] W. Birkfellner, M. Figl, C. Matula, J. Hummel, R. A. Hanel, H. Imhof, W. Piller, F. Wanschitz, A. Wagner, F. Watzinger, and H. Bergmann, "Stereoscopic visualization in the varioscope AR: A see-through head-mounted display for surgical navigation," *Proc. SPIE Med. Imag.*, vol. 4681, pp. 425–435, 2002.